Journal of Materials Chemistry A

Accepted Manuscript

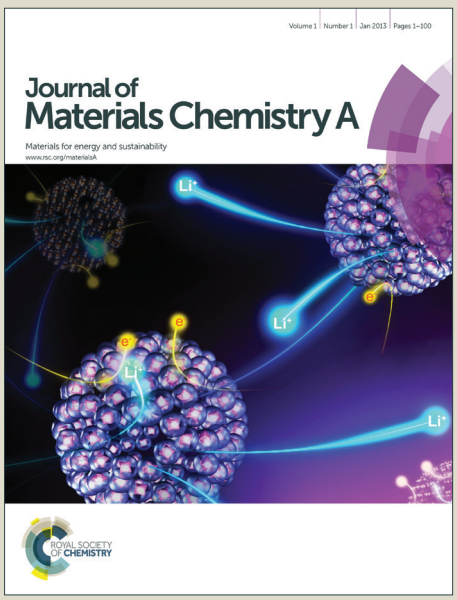

ROYAL SOCIETY OF CHEMISTRY

www.rsc.org/materialsA

Journal Name

RSCPublishing

ARTICLE

High Photocurrent Generation by Photosystem I on Artificial Interfaces Composed of π-System-Modified Graphene

S.C. Feifel,[a,*] K.R. Stieger,[a] H. Lokstein,[b] H. Lux[c] and F. Lisdat[a]

Cite this: DOI: 10.1039/x0xx00000x

Received 00th January 2012,
Accepted 00th January 2012

DOI: 10.1039/x0xx00000x

www.rsc.org/

Photosystem I (PSI) is a key component of the oxygenic photosynthetic electron transport chain because of its light-induced charge separation and electron transfer (ET) capabilities. We report the fabrication of an efficient graphene-biohybrid light-harvesting electrode consisting of cyanobacterial trimeric PSI complexes immobilized onto π-system-modified graphene electrodes. Based on the strong interaction between conjugated aromatic compounds and the graphene material via π-π-stacking, we have designed a simple but smart platform to fabricate light-driven photoelectrochemical devices. Due to the possibility of surface property adaptation and the excellent conductivity of graphene, the modified biohybrid electrodes exhibit a well-defined photoelectrochemical response. In particular, the PSI-graphene electrode applying pyrene butyric acid *NHS* ester display a very high photocurrent output of 23 μA/cm^2 already at the open circuit potential which can be further increased by an overpotential and the use of an electron acceptor (methyl viologen) under air saturation up to 135 μA/cm^2. Comparing the graphene-PSI biohybrid systems based on different π-system-modifiers reveals that the pyrene derivatives result in higher current outputs compared to the anthracene derivatives and that the covalent fixation during immobilization appears more efficient compared to simple adsorption.

Interestingly, the pyrene-based PSI electrodes also display a nearly unidirectional photocurent generation, establishing the feasibility of conjoining these nanomaterials as potential constructs in next-generation photovoltaic devices.

Introduction

Graphene, first reported in 2004, is still a concerned star on the horizon of nanosized material science.[1,2] The strictly two-dimensional material exhibits exceptionally high crystal and electronic quality, and despite its short history, has already revealed a superfetation of potential applications. The unique physiochemical and structural properties of graphene such as high electrical and thermal conductivities,[1,3,4] good transparency,[5] mechanical strength,[6,7] and inherent flexibility[8] of single-graphene sheets have led to developments in several technological fields, such as microelectronic and optoelectronic devices,[2,9,10] nanoelectronics,[11] electrocatalysis,[12,13] polymer composites,[14] transparent conductors,[15] and energy storage materials.[16,17] Different but similarly fascinating properties are exhibited by double-, and multilayer graphene.[18-20]

Covalent or noncovalent chemical functionalization[21] can render normally-inert graphene chemically sensitive, which is critical for applications as sensing interface.[22] An introduction of functional groups on graphene is often necessary for the assembly of biomolecules. The graphene surface can be modified by several methods. If a non-invasive approach is desired without affecting the properties of graphene molecular self-assembly by π-π-stacking is an elegant option.[23-27] Thereby grafted functionalities can be either used for electrostatic and/or covalent fixation of the desired biomolecules onto the graphene surface.

Not only graphene has attracted strong attention of the scientific community but also the efficiency of natural energy converting processes,[28-31] whereby the oxygenic photo-synthesis is by far the most important one, notably, since this process requires only water and sunlight as sources to be converted into chemical energy.[29,32] Photosynthesis can be considered a source of inspiration for the development of technologies which may help to harness solar power for energy demands beyond fossil fuels. In particular the two photosystems (PS) of the oxygenic photosynthesis have been used to construct new hybrid solar energy-converting systems.[33-35]

In the cyanobacterium *Thermosynechococcus elongatus* (*T. elongatus*), PSI is a trimeric pigment-protein super-complex with 12 different protein subunits, harbouring 96 chlorophylls a (Chl *a*) – per monomeric subunit. Most Chls serve as light-harvesting antenna pigments and 6 Chls form the electron transport chain.[36] Electron transfer (ET) in PSI starts at a luminal pigment dimer, Chl *a*/Chl *a'* (P700) ultimately leading to a reduction of the stromal located terminal iron-sulfur-cluster (FB).[37,38]

PSI can be readily isolated from plants and cyanobacteria with a high yield.[37,38,40] Moreover, in PSI absorption of light results in charge separation with a quantum efficiency of nearly

unity.[39] Thus PSI is frequently used as a natural resource for development of light converting devices.[37,38,40] Besides the light-to-current conversion, the charge separation of PSI is likely to be used for light-driven redox and/or enzymatic reactions, in which the electrons may be used to power enzymatic conversions. In such systems efficient coupling of PSI with electrodes and/or conducting interfaces is essential. That an efficient coupling of proteins and enzymes is essential for a productive ET has been shown before with redox protein or enzyme-based electrodes.[41,42]

PSI has been assembled onto a variety of different substrates, including gold, ITO, ZnO, TiO_2.[43-45] On this basis several developments have enabled improvements in the photo-generated currents that can be produced by PSI-electrode based devices.[44,46-49] These improvements include novel PSI immobilization methods on gold electrodes,[50–53] embedding PSI within polymer matrices,[54] the use of thick protein films,[46] the use of semiconductor electrode materials[44,45] and directed assembly of PSI on a biomolecular platform (e.g. cytochrome *c*; cyt *c*).[55] The use of carbon nanostructures such as graphene with biomolecules to develop nanocomposite materials has become an area of great research interest.[56,57] The integration of PSI with carbon nanomaterials, however, is rather limited. One approach demonstrated how PSI is covalently attached to carbon nanotubes.[58,59] PSI can also be interfaced on a graphene electrode via drop coating, resulting in rather small and undefined currents – especially at the open-circuit potential almost no photocurrent has been displayed by this approach.[60] Here we describe how the directed assembly of PSI on π-system modified graphene leads to a remarkable enhanced unidirectional photocurrent generation.

Results and Discussion

We hypothesized that interfacing PSI with a graphene electrode modified with π-stacking compounds carrying functional groups would lead to an improved organization and orientation of PSI on the surface, and thus improve the electron transfer and photocurrent generation. Therefore, the influence of various graphene electrode surface modifications on PSI assembly and photoelectrochemistry has been investigated. In Fig. 1 the basic principle of such architecture is schematically shown.

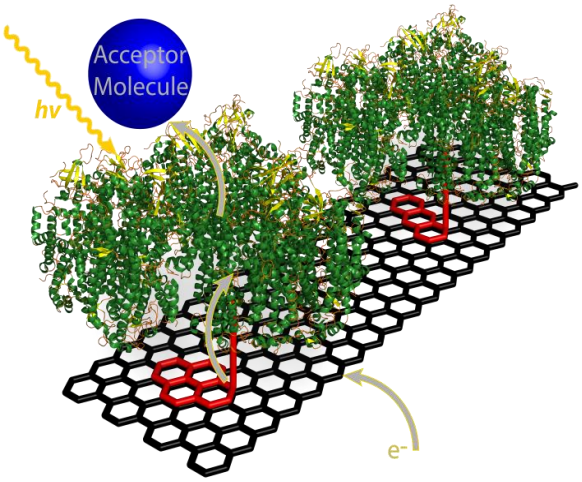

Fig. 1 Schematic depiction of a graphene/π-system/PSI-based electrode. For example two different π-systems are shown: pyrene- and anthracene-based one; featuring a covalent or electrostatic fixation of PSI, respectively. Arrows indicate the electron flow through this nanobionic architecture.

The graphene electrodes used in this study have been constructed and characterized as follows: Graphene has been deposited on a polished silicon wafer with 300 nm thermally grown SiO_2 by filtered High Current Arc (Φ-HCA) in noble gas atmosphere. The coating consists of mostly flat graphene-flakes with a thickness of about 2 nm. This has been verified by optical measurements such as Raman spectroscopy and spectrophotometry indicating a thin graphene coating with 81% transmission and a thickness of about 5-8 layers (Fig. S1). Detailed information on the graphene deposition process is given in the Electronic Supporting Information (ESI).

Photoelectrochemical investigations of PSI/π-system modified graphene electrodes

In our study we have used graphene as a base material. In order to adopt the surface properties in a non-invasive fashion for a proper assembly of PSI we modified the surface with different aromatic compounds: pyrene and anthracene derivatives. The chosen π-system structures differ in their aromatic skeleton but also in their substitution pattern, i.e., the functional groups they carry. The π-systems by themselves are in turn supposed to assemble on the graphene surface via π-π-stacking interactions. PSI is assembled on the modified electrodes by incubation for 48 h (see ESI). The various structures and their nomenclature are given in Fig. 2.

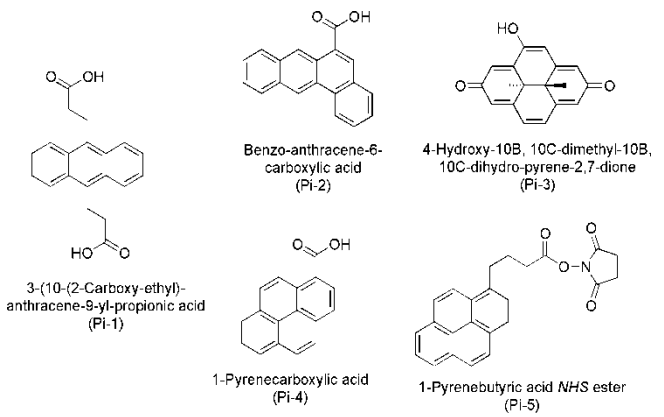

Fig. 2 Structures and nomenclature of the used and investigated π-systems for the directed assembly of PSI onto graphene electrodes.

In order to study the functional properties of the different π-system-modified graphene-PSI composite electrodes, we perform photochronoamperometric experiments and chopped-light voltammetry (CLV) with and without an additional acceptor molecule, methyl viologen (MV^{2+}) under air saturation.

In previous reports it was shown that graphene by itself can cause a photo-induced current upon illumination.[48] On account of this, we first tested in a series of control experiments the π-system-modified graphene electrodes for possible photocurrent generation. Apparently, no photocurrent can be observed when the π-system-modified graphene electrodes are investigated at their open circuit potential (OCP) and illuminated by low light intensities. When large overpotentials (-600 mV vs. OCP) and high light intensities (100 mW cm^{-2}) are applied a poor photocurrent can be observed for some of the π-system

modified graphene electrodes (Fig. S2). These values have been taken into account and subtracted from the photocurrent values which are given in Table 1. In general these values are at least a factor of seven smaller compared to the merest photocurrents observed for the π-1 & π-2-based PSI-electrodes and 3-4 orders of magnitude smaller than the current densities observed for the π-5-based biohybrid system.

In addition, it needs to be mentioned that the bare/unmodified graphene electrodes have been investigated regarding their ability to work as an assembly platform of PSI. It has been found that only a very small amount of PSI binds to the graphene surfaces (which will be discussed in more detail in one of the following sections), and that no significant photocurrent generation can be seen. This may underline that the π-systems carrying functional groups are of vital importance for the assembly process of functional PSI.

Photoelectrochemistry – PSI/anthracene-based graphene electrodes.

For this investigation two different π-systems based on an anthracene aromatic scaffold are studied for the assembly of PSI. One of them (π-2), possesses two carboxyl-groups and its aromatic scaffold is a linear condensed aromatic skeleton with three rings, whereby the other (π-1) owns only one carboxyl-group and its aromatic scaffold is composed of four rings. Both anthracene-based electrodes behave almost similar; they display rather small and bidirectional photocurrents. For example the π-1-based PSI electrode displays a comparatively weak cathodic photocurrent at OCP (-150 mV vs. Ag/AgCl), with a current density of 130 nA/cm^2 at a light intensity of 100 mW cm^{-2} (Fig. 3). Electron flow can be explained in this architecture as follows: the excited PSI can take electrons from the electrode and thus the oxidized reaction centre of PSI is reduced. Furthermore the electrons are transfer from the excited luminal side of PSI to the stromal side where the electrons are used to reduce oxygen or the additional electron acceptor MV^{2+}.

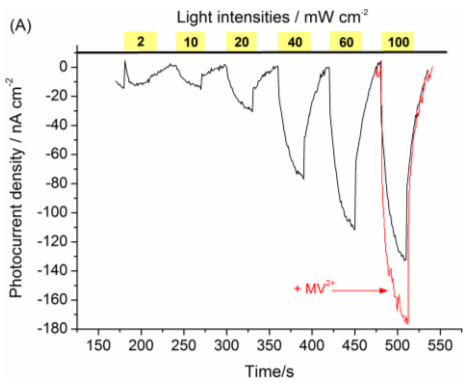

Fig. 3 Photochronoamperometric measurements of a graphene/carboxyl-anthracene(π-1)/PSI electrode at different light intensities (2, 10, 20, 40, 60, 100 mW cm^{-2}). Measured at OCP (-150 mV vs. Ag/AgCl); overlay (red line): addition of MV^{2+} (250 µM). Measurements are performed under air saturation.

The addition of MV^{2+} results in an improved photocurrent output (170 nA/cm^2). As the reaction of PSI with molecular oxygen as electron acceptor is rather slow; the addition of MV^{2+} leads to an enhanced electron withdrawal at the stromal side from the excited protein. This results in an increased photocurrent output if no other processes are limiting.

However, the currents generated by both systems seem to be rather unstable and no sharp induction of the current can be seen when the light is turned on (Fig. 3, S3). A necessary comment to these systems is that at low light intensities (<10 mW cm^{-2}) almost no photocurrent is displayed – not at the OCP and also not at small overpotentials. At higher light intensities (100 mW cm^{-2}) and an overpotential of -100 mV vs. OCP the cathodic photocurrent density can be enhanced to 240 nA/cm^2. Chopped light voltammetric measurements depict that already at rather small overpotentials the current cannot be enhanced any further (Fig. S3). It should be noted that for all investigated modifications at least 3 electrodes have been prepared and assessed. Table 1 collects the photocurrent values for all of the tested PSI electrodes.

The photoelectrochemical behaviour shows, that the surface modification via the anthracene-derivatives is suited to promote the assembly of PSI and also to connect the protein with the electrode. However, the efficiency is not very high for both anthracene-based PSI electrodes. It seems that the PSI electrode interaction becomes rate limiting and that the system is not limited by the electron withdrawal. The chopped light experiments also reveal that cathodic and anodic photocurrents are displayed (Fig. S3). This means that the PSI supercomplex is assembled in two ways on the electrode. If cathodic currents are displayed the luminal side of PSI is faced to the electrode surface and from anodic currents it can be concluded that the stromal side of PSI is faced to the transducer surface. The recorded anodic current is considerably smaller as the cathodic one, indicating a productive orientation of PSI on these π-1/π-2-based systems. However, it seems that also a large fraction of the protein complex is disorderly assembled. Hereby different possibilities for the connection with the electrode exist which hinders a defined photoelectrochemical response.

Photoelectrochemistry – PSI/pyrene-based graphene electrodes.

Three different pyrene-based π-systems are selected (Fig. 2). These systems differ in their substitution pattern and the kind of interactions they can cause to PSI. π-3 carries a hydroxyl-, a methyl, and two keto-groups, which in turn are supposed to form hydrogen bonds to PSI and/or non-polar interactions. π-4 carries only one carboxyl-group for hydrogen bonding/ electrostatic interactions and the reactive *NHS*-ester group of π-5 is supposed to form a covalent bond with one of the lysine side chains of PSI.

Graphene/hydroxyl-keto-pyrene (π-3)/PSI electrode:

First, PSI has been assembled onto hydroxyl-keto-pyrene/graphene electrodes and the photocurrent generation at the OCP (-150 mV vs. Ag/AgCl) is assessed at different light intensities (2 – 100 mW cm^{-2}). For low intensities a rather weak cathodic photocurrent has been observed. When light intensities are increased up to 100 mW cm^{-2}, the photocurrent is more defined and the current density is raised up to 750 nA/cm^2 (Fig. 4). Upon the addition of MV^{2+} the photocurrent can be stabilized and enhanced. In case of an applied overpotential of -100 mV vs. OCP the photocurrent generation can be further improved to a certain extend (1.6 µA/cm^2), but still seems not well defined. Also the addition of MV^{2+} (250 µM) at this overpotential does not result in a significant improvement of both: photocurrent output and stability (Fig. S4).

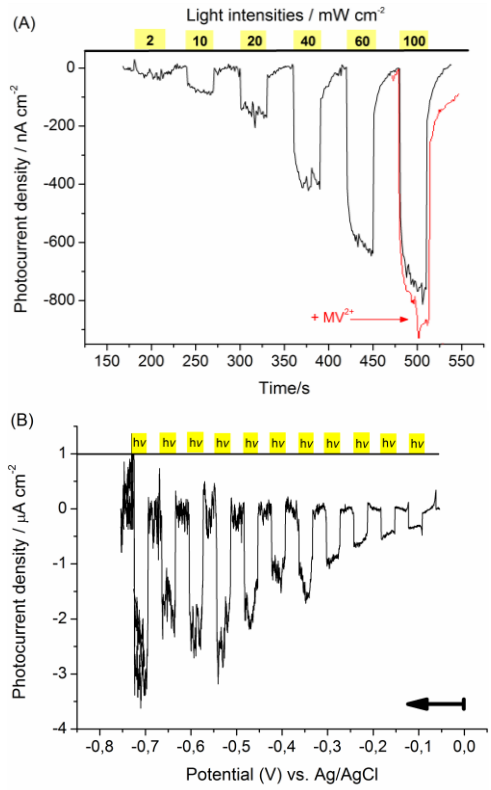

Fig. 4 (A) Photochronoamperometric measurements of a graphene/hydroxyl-keto-pyrene (π-3)/PSI electrode at different light intensities (2, 10, 20, 40, 60, 100 mW cm^{-2}), measured at OCP (-150 mV vs Ag/AgCl); overlay (red line): addition of MV2+ (250 µM). B) Chopped light voltammetry measurements at a constant light intensity of 60 mW cm^{-2} with a scan rate of 2 mV/s. Measurements are performed under air saturation.

These observations are corroborated by the chopped light voltammetric experiments (Fig. 4B), whereas the photocurrent output reaches a plateau at a potential of -550 mV vs. Ag/AgCl (-400 mV vs. OCP). At this point the addition of MV^{2+} does not lead to a significant improvement of the current densities, but causes a stabilization of the current. Since here the enhanced withdrawal of electrons from PSI (by the faster reaction of MV^{2+} with the terminal F_B-cluster) does not significantly enhance the current, it becomes clear that the PSI communication with the electrode tends to limit the current flow through the whole system. An overview of the photo-current values is given in Table 1.

Graphene/carboxyl-pyrene (π-4)/PSI electrode:
For the carboxyl-pyrene-PSI (π-4) electrodes rather small cathodic photocurrents are displayed at OCP (-180 mV vs. Ag/AgCl) applying low light intensities <10 mW cm^{-2} (Fig. 5). At higher light intensities the current is enhanced quite significantly (570 nA/cm^2), and even further by the addition of MV^{2+} (875 nA/cm^2). The strongest impact on photocurrent magnitude and photocurrent stability however, is seen if an overpotential is applied (Figure 5). Thus at -100 mV vs. OCP a valuable improvement is found (1.7 µA/cm^2). This can be even raised up to 7.3 µA/cm^2 at larger overpotentials improving the photocurrent remarkably by a factor of twelve compared to the current at OCP (Fig. S5).

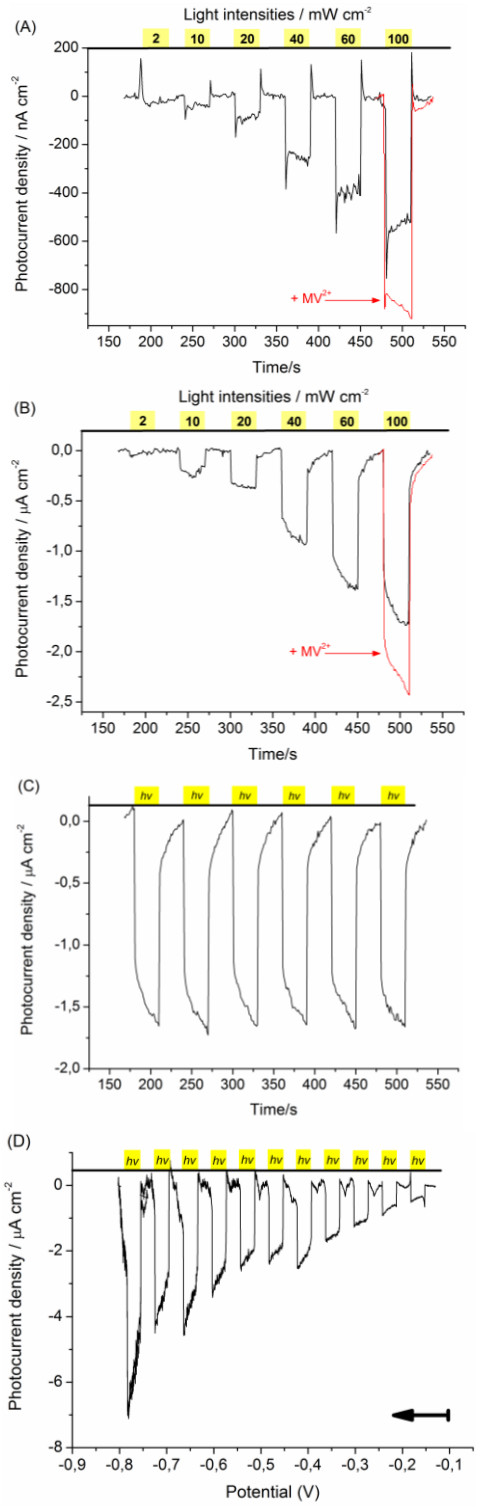

Fig. 5 Photochronoamperometric measurements of a graphene/carboxyl-pyrene (π-4)/PSI electrode at different light intensities (2, 10, 20, 40, 60, 100 mW cm^{-2}). A) Measured at OCP (-180 mV vs Ag/AgCl); overlay (red line): addition of MV^{2+} (250 µM). B) Measured at an overpotential (-280 mV vs Ag/AgCl); overlay (red line): addition of MV^{2+} (250 µM). C) At an overpotential (-280 mV vs Ag/AgCl) with a constant light intensity of 60 mW cm^{-2}. D) Chopped light voltammetry measurement at a constant light intensity of 60 mW cm^{-2} with a

scan rate of 2 mV/s. Measurements are performed under air saturation.

CLV measurements additionally punctuate these observations, as we see an increase of photocurrent up to a potential of -800 mV vs. Ag/AgCl, which is further improved due to the addition of MV^{2+} (Fig. 5).
These results indicate an efficient and unidirectional electron transfer between the excited PSI and the electrode. Thereby it has been demonstrated that even such large and sophisticated protein complexes can be assembled in a productive way for effective heterogeneous electron transfer. Hence this architecture is quite a well functioning example for a potential-dependent photodiode on the basis of PSI-graphene hybrids. A compilation of the values is given in Table 1.

Graphene/pyrene butyric acid NHS ester (π-5)/PSI electrode:
An enormous improvement in photocurrent generation and photocurrent stability is found for the covalent approach tested within this study by the use of the π-5 compound. This is valid in comparison to the systems investigated within our study but also to previously published reports on PSI/carbon electrodes.[45,60-63] Here a photocurrent density of 23 μA/cm^2 is already reached at OCP (-260 mV vs. Ag/AgCl) at a light intensity of 100 mW cm^{-2}. But also at low light intensities a significant and stable current is obtained (Fig. 6).

Photocurrent values at OCP are in the majority not given in previous studies on PSI-based electrodes.[45,60-63] This is because most of the to date reported systems do not furnish a viable photocurrent generation without applying a driving force.
The photocurrent output for this system can be significantly enhanced by the addition of MV^{2+} (250 μM) at OCP by ~90 % (39 μA/cm^2) as well as by applying a slight overpotential of -90 mV vs. OCP (49 μA/cm^2) Fig. S6. This means that in this case the PSI-electrode communication is so efficient that the withdrawal of electrons from the excited PSI is limiting the efficiency of the system. The chopped light voltammetric experiments support these findings (Fig. 6, S6). As a result of an applied overpotential and the addition of MV^{2+} the photocurrent output can be even raised up to 135 μA/cm^2. Additionally, the photocurrents generated by this system are very stable in comparison to the other investigated π-system based electrodes and published data. This is valid for longer time periods of measurements, multiple use of the electrode, but also for storage of the photohybrid electrode, since after two weeks still at least 50 %, and after half a year 40 % of the activity is retained (Fig. S6). A detailed record of the photocurrent data is compiled in Table 1.
In addition it should be pointed out here, that for the current density evaluation only the steady-state current values under illumination are used and not the photocurrents after switching-on the light, to give reasonable values (such misleading photocurrents have been repeatedly reported[45,60-63]).

Not less important, especially with respect to the remarkable photocurrent at OCP, is the direction of the ET of this system, as exclusively a cathodic photocurrent has been observed. Thereby, suggesting a unidirectional ET pathway with a preferred orientation of PSI on the modified graphene interface. This is a clear achievement since the rather complex membrane protein trimer has many interaction sites. An orientation during the surface binding process is however essential for an efficient current output, as ET in PSI is unidirectional form the luminal to the stromal side.

As a continuative characterization the light power dependence has been evaluated for the π-5-based electrode. If light is considered as a substrate for PSI one can use the Michaelis-Menten kinetics to calculate an apparent K_M value[61] (Fig. 6), even if the fits are not accurate for very low light intensities (which has also been observed with other PSI-electrode strategies[55]).

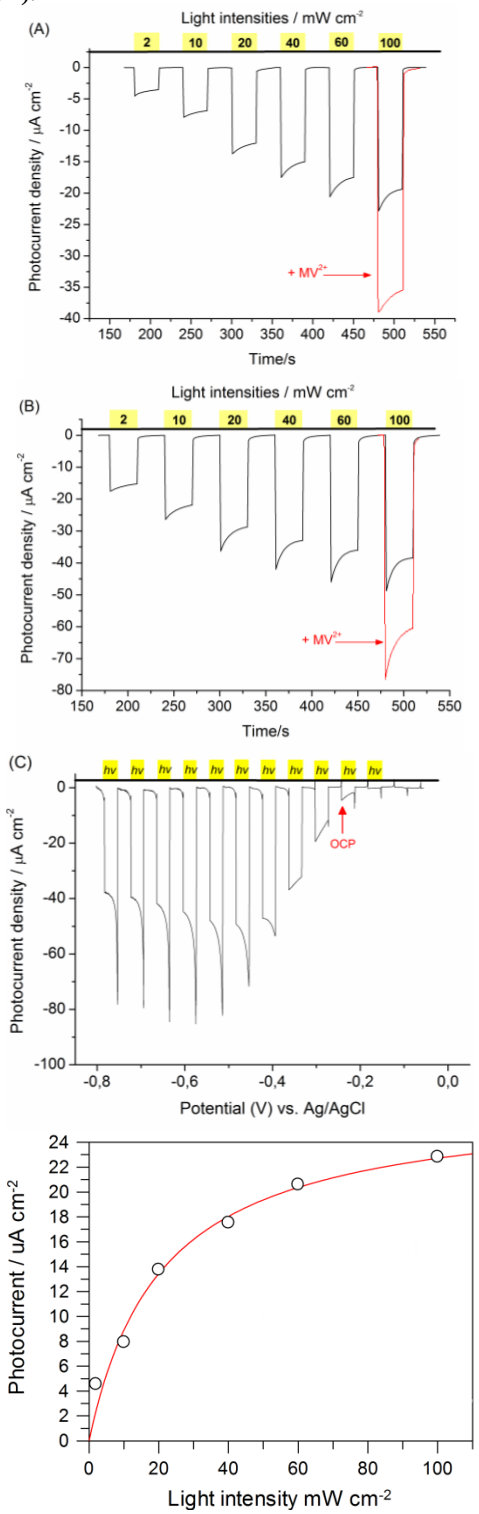

Fig. 6 Photochronoamperometric measurements of a graphene/*NHS*-pyrene (π-5)/PSI electrode at different light intensities (2, 10, 20, 40, 60, 100 mW cm^{-2}). A) Measured at

OCP (-260 mV vs Ag/AgCl); overlay (red line): addition of MV^{2+} (250 µM). B) Measured at an overpotential (-350 mV vs Ag/AgCl); overlay (red line): addition of MV^{2+} (250 µM). C) Chopped light voltammetry measurements at a constant light intensity of 60 mW cm^{-2} with a scan rate of 2 mV/s. Measurements are performed under air saturation. D) Michaelis-Menten plot of the π-5-based electrode at OCP (-260 mV vs Ag/AgCl). Red curve indicates the fit for determination of the apparent K_M-value.

A quite strong impact on the K_M-value can be seen due to the applied electrode potential. From the fit parameters a maximum photocurrent density of 23 µA cm^{-2} and a K_M of 20±1 mW cm^{-2} (n = 3) can be derived at OCP. But if an overpotential of -90 mV vs. OCP is applied the K_M decreases significantly to 6.3±0.2 mW cm^{-2}. This trend continues up to an overpotential of -190 mV vs. OCP (K_M = 1.6 ±0.1 mW cm^{-2}). Since the change in K_M goes along with an increase in I_{max} it indicates a distinctly efficient light-to-current conversion of the absorbed light. This in turn highlights once again the outstanding properties of the π-5-based photobioelectrode.

It needs to be added, that the photocurrent density and unidirectionality of ET of the graphene-π-5-PSI electrode outperforms by far previously published studies on carbon-based PSI electrodes, particularly at OCP.[45,60-63] Another system which is based on a redox hydrogel-PSI architecture,[64] even if it is more like a multilayer arrangement can be compared with our system. In this study also a high photocurrent (43 µA cm^{-2}) has been achieved at OCP. However it has to be pointed out that our system is most likely a PSI-monolayer arrangement facilitating DET onto a graphene-electrode, where at the other system is based on a bulk immobilization (multilayer-like) and applying a mediator for ensuring electron transfer.

PSI assembly process on π-system modified graphene QCM chips.

On the basis of the photoelectrochemical experiments alone, one cannot elucidate whether the overall amount of PSI deposited on the electrode surface is influenced by the change in the π-system. To gain further insight into the quite significant disparities in photocurrent output by the use of various π-systems, the most promising and interesting systems (π-4 and π-5) have been studied by Quartz crystal microbalance (QCM) to elucidate how the π-system structure influences the assembly of PSI. Prior to the QCM measurements, graphene-like carbon is deposited on the quartz chips using the method as before to provide alike surfaces on the chips as on the graphene electrodes. These chips are then modified according the described procedure for graphene electrodes.

After the surface has been modified by the respective π-system a solution of PSI is flushed at a defined flow rate over the chip (ESI). The assembly process for which the carboxyl-substituted pyrene (π-4)/graphene chip is used, shows a clear adsorption behaviour of PSI accompanied by a well detectable mass accumulation of Δf = 60±4 Hz at pH 7 (Fig. S8). The following flush with buffer leads only to a small change in signal because of a small degree of PSI desorption (~4 Hz).
In the same manner the NHS activated pyrene (π-5) has been studied (Fig. S9). Interestingly, for this π-5 modified surface a stronger protein adsorption has been observed accompanied by a very high mass accumulation (PSI, Δf = 330±5 Hz). Moreover, during the adjacent rinsing step with buffer virtually no signal change has been observed. This, in turn, indicates that the PSI complexes interact productively with the surface and are stably bound. The results are corroborated by experiments in which additional rinsing steps with a buffer of high ionic strength do not cause a significant change in signal. In the case of an electrostatically adsorpt protein such high ionic strength would lead to desorption of the protein from the surface as the required charges are masked by the high concentration of counter ions. In reverse this observation is highly indicative that the π-5-based electrode has lead via the reaction of the *NHS*-ester to a covalent fixation of PSI.

The difference in polarity of these two pyrene-based surfaces has been verified by contact angle (CA) investigations. Here it has been found that the contact angle for the π-4 modified graphene (86±3°) is lower than for the π-5 modified interface (106±2°). This is consistent with the respective functional groups.

Supportingly, it needs to be mentioned, that the adsorption process of PSI on unmodified graphene has also been investigated by QCM (Fig. S7). It has been found that only a small degree of non-specific binding to the bare graphene surface occurs with a signal change of about Δf = 9±2 Hz. This is accompanied by a very hydrophobic surface as has been verified by CA measurements (119±4°). Thus, the functionalized π-systems are indeed needed to pursue a specific assembly and orientation of PSI. On the basis of the QCM experiments and the photoelectrochemical investigations, one can clearly conclude that the mass deposition during the assembly process for the investigated π-system/PSI assemblies can be correlated to the amount of electro-active PSI and, thus, to the magnitude of the respective photocurrent generation.

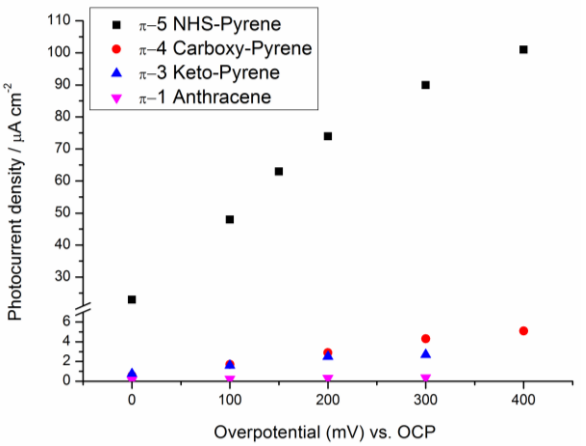

Fig. 7 Photocurrent dependency on the applied overpotential of different graphene•π-system/PSI electrodes.

The chemical nature of the π-substance used is governing the interaction of the pigment-protein complex with the surface. Fig. 7 compiles the behaviour of the different PSI-based electrodes investigated in this study and demonstrates the different efficiency in photocurrent generation as well as the different ability of the systems to follow the applied potential. A direct covalent coupling during the interaction process seems to be favourable with respect to the amount of PSI, a preferred PSI orientation and, thus, a unidirectional and potential-controlled photocurrent generation. From a rational point of view one may expect that the adsorptive approaches should lead to a favourable orientation of the PSI complexes on the modified interface, and thus, to higher photocurrents. However, the covalent fixation outperforms the other investigated approaches by far. Taking also the contact angle measurements

into account, a certain balance between hydrophobic/hydrophilic properties seems to be favourable during PSI deposition for a proper orientation of PSI to induce a directional electron transfer. Covalent binding is obviously beneficial to retain this configuration for a large number of PSI molecules. While the exact structure of the PSI complexes on the π-system modified surface remains open to future investigations, it should be noted that the results are consistent with the proposed assembly of the PSI trimers on the pyrene modified graphene, preferentially with the luminal side down.[36,65,66]

Conclusions

We have successfully constructed new graphene-based photohybrid electrodes composed of PSI and π-system-modified graphene. The specific adsorption of PSI on these π-system-modified graphene interfaces leads to a significant improvement of the photocurrents generated at the open circuit potential as well as for an reasonable overpotential window (-100 to -200 mV vs. OCP) in comparison to previously published reports on PSI-carbon electrodes. Whereas anthracene modifiers result in an appearance of anodic and cathodic photocurrents the pyrene-based systems exclusively display a unidirectional cathodic photocurrent, indicating a directed assembly of PSI with the luminal side down.

Comparing the modified graphene systems based on the pyrene-modifiers one can state that the covalent approach (π-5) is the most effective one. The photocurrent density particularly at OCP, but also at different overpotentials is the highest. The improvements are likely attributed to a higher mass deposition of PSI on these electrodes, which originates from specific interactions with the π-system-modified interface. But the pure adsorption with (π-4) also provides a feasible way to assemble a stable PSI layer.

By the addition of an electron acceptor (MV^{2+}) the photocurrent output can be even further raised significantly for the π-4 and π-5-based PSI electrodes. The photocurrents are found to be rather stable for both architectures but on basis of the covalent one (π-5), a tremendous improvement has been established: the photocurrent is stable over longer measuring periods, multiple use of the electrode, as well as after storage of the electrode. Based on the ratio of cathodic to anodic photocurrent it can be concluded that the pyrene-π-system modified PSI electrodes exhibit a photo-diode like behaviour.

The advantage of coupling PSI to the modified graphene via covalent binding (π-5) is also reflected by the light-power dependency study which indicates a distinctly efficient current conversion of the consumed light.

These results demonstrate the potential of integrating modified-π-systems with graphene-based electrodes for functional and directional PSI assembly. More broadly, this systematic study reveals how modified π-π-stacking molecules can be used to tune the surface properties but also allow a stable fixation while guaranteeing an efficient interaction of graphene with the biomolecular complex. These benefits can not only be used in photobioelectrocatalytic systems but also in systems where light is applied to drive reaction schemes for synthesis.

Table 1 Photocurrent responses at OCP and different overpotentials with and without MV^{2+} for all graphene-π-system-PSI electrode architectures.

Graphene ΠI-Sys./PSI electrodes	Architecture OCP[a)]	Photocurrent at OCP[a)]	Photocurrent at OCP[a)] + MV^{2+} [b)]	Photocurrent at over potential of 100 mV[c)]	Photocurrent at over potential of 200 mV[c)]	Photocurrent at over potential of 300 mV[c)]	Photocurrent at over potential of 400 mV[c)]	Photocurrent at over potential of 300 mV[c)] + MV[b)]
1	-150 mV	130±10 nA	170±10 nA	240±5 nA	320±8 nA	360±4 nA	n.d.	480±5 nA
3	-150 mV	750±10 nA	840±5 nA	1.6±0.2 µA	2.5±0.1 µA	2.7±0.1 µA	n.d.	2.9±0.2 µA
4	-180 mV	570±10 nA	875±5 nA	1.7±0.1 µA	2.9±0.2 µA	4.3±0.1 µA	5.1±0.3 µA	7.3±0.5 µA
5	**-260 mV**	**23±0.5 µA**	**39±0.7 µA**	**49±0.4 µA**	**75±1 µA**	**90±2 µA**	**102±3 µA**	**135±5 µA**

[a)]Open circuit potential; [b)]250 µM; [c)]vs. OCP.

Acknowledgements

This research was financially supported by the Bundesministerium für Bildung und Forschung BMBF, Germany (Biotechnologie 2020+, projects: 031A154A+B). The authors are grateful to A. Kapp for technical assistance and thankful to Johnannes Gladisch for the preparation of the conceptual figure in this manuscript.

Notes and references

[a] Biosystems Technology, Technical University of Applied Sciences Wildau, Hochschulring 1, 15745 Wildau, Germany. *E-mail: feifel@th-wildau.de; Fax: +49-3375-508-458; Tel: +49-3375-508-158.*

[b] Institute of Molecular, Cell & System Biology, University of Glasgow, 120 University Place, G12 8TA, Scotland.

[c] Photonics, Technical University of Applied Sciences Wildau, Hochschulring 1, 15745 Wildau, Germany.

† Electronic Supplementary Information (ESI) available: Experimental procedures, characterization data, additional QCM and photoelectrochemical data. See DOI: 10.1039/b000000x/

1 K. S. Novoselov, A. K. Geim, S. V. Morozov, D. Jiang, Y. Zhang, S. V. Dubonos, I. V. Grigorieva, A. A. Firsov, *Science*, 2004, **306**, 666.

2 A. Geim, K. Novoselov, *Nat. Mater.*, 2007, **6**, 183.

3 J. H. Chen, C. Jang, S. D. Xiao, M. Ishigami, M. S. Fuhrer, *Nat. Nanotechnol.*, 2008, **3**, 206.

4 A. A. Balandin, S. Ghosh, W. Z. Bao, I. Calizo, D. Teweldebrhan, F. Miao, C. N. Lau, *Nano Lett.*, 2008, **8**, 902.

5 R. R. Nair, P. Blake, A. N. Grigorenko, K. S. Novoselov,T. J. Booth, T. Stauber, N. M. R. Peres, A. K. Geim, *Science*, 2008, **320**, 1308.
6 C. Lee, X. D. Wei, J. W. Kysar, J. Hone, *Science*, 2008, **321**, 385.
7 Bunch, J. S., et al., *Science*, 2007, **315**, 490.
8 M. D. Stoller, S. J. Park, Y. W. Zhu, J. H. An, R. S. Ruoff, *Nano Lett.*, 2008, **8**, 3498.
9 F. Bonaccorso, Z. Sun, T. Hasan, A. C. Ferrari, *Nat. Photonics* 2010, **4**, 611.
10 G. Eda, M. Chhowalla, *Adv. Mater.*, 2010, **22**, 2392.
11 J. S. Wu, W. Pisula, K. Müllen, *Chem. Rev.*, 2007, **107**, 718.
12 D. Chen, L. H. Tang, J. H. Li, *Chem. Soc. Rev.*, 2010, **39**, 3157.
13 H. Bai, Y. X. Xu, L. Zhao, C. Li, G. Q. Shi, *Chem. Commun.*, 2009, 1667.
14 S. Stankovich, D. A. Dikin, G. H. B. Dommett, K. M. Kohlhaas,E. J. Zimney, E. A. Stach, R. D. Piner, S. T. Nguyen, R. S. Ruoff, *Nature*, 2006, **442**, 282.
15 J. K. Wassei, R. B. Kaner, *Mater. Today*, 2010, **13**, 52.
16 Q. Wu, Y. X. Xu, Z. Y. Yao, A. R. Liu, G. Q. Shi, *ACS Nano*, 2010, **4**, 1963.
17 E. Yoo, J. Kim, E. Hosono, H. Zhou, T. Kudo, I. Honma, *Nano Lett.*, 2008, **8**, 2277.
18 B. Partoens, F. M. Peeters, *Phys. Rev. B*, 2006, **74**, 404.
19 S. V. Morozov, et al. *Phys. Rev. B*, 2005, **72**, 201401.
20 Y. Zhang, J. P. Small, M. E. S. Amori, P. Kim, *Phys. Rev. Lett.*, 2005, **94**, 176803.
21 V. Georgakilas, M. Otyepka, A. B. Bourlinos, V. Chandra, N. Kim, K. C. Kemp, P. Hobza, R. Zboril, K. S. Kim, *Chem. Rev.*, 2012, **112**, 6156.
22 A. K. Geim, *Science*, 2009, **324**, 1530.
23 J. M. MacLeod, F. Rosei, *Small*, 2014, **10**, 1038.
24 A. Rochefort, J. D. Wuest, *Langmuir*, 2008, **25**, 210.
25 A. AlZahrani, *Appl. Surf. Sci.*, 2010, **257**, 807.
26 Y.-H. Zhang, K.-G. Zhou, K.-F. Xie, J. Zeng, H.-L. Zhang, Y. Peng, *Nanotechnol.*, 2010, **21**, 065201.
27 S. M. Kozlov, F. Viñes, A. Görling, *Carbon*, 2012, **50**, 2482.
28 J. F. Turrens, *J. Physiol.*, 2003, **552**, 335.
29 A. N. Glazer, A. Melis, *Annu. Rev. Plant Physiol. Plant Mol. Biol.*, 1987, **38**, 11.
30 P. S. Brookes, A. L. Levonen, S. Shiva, P. Sarti, V. M. Darley-Usmar, *Free Radic. Biol. Med.*, 2002, **33**, 755.
31 G.W. Brudvig, R. H. Crabtree, *Proc. Natl. Acad. Sci. USA*, 1986, **83**, 4586.
32 P. J D. Janssen, M. D. Lambreva, N. Plumere, C. Bartolucci, A. Antonacci, K. Buonasera, R. N. Frese, V. Scognamiglio, G. Rea, *Front. Chem.*, 2014, **2**, 36.
33 A. Badura, T. Kothe, W. Schuhmann, M. Rögner, Energy Environ. Sci., 2011, **4**, 3263.
34 C. F. Meunier, X.-Y. Yang, J. C. Rooke, B.-L. Su, ChemCatChem, 2011, **3**, 476.
35 F. Wang, X. Liu, I. Willner, *Adv. Mater.*, 2013, **25**, 349.
36 P. Jordan, P. Fromme, H. T. Witt, O. Klukas, W. Saenger, N. Krauss, *Nature*, 2001, **411**, 909.
37 I. Grotjohann, P. Fromme, *Photosynth. Res.*, 2005, **85**, 51.
38 A. Diaz-Quintana, W. Leibl, H. Bottin, P. Setif, *Biochemistry*, 1998, **37**, 3429.
39 N. Nelson, C. F. Yocum, *Annu. Rev. Plant Biol.*, 2006, **57**, 521.
40 H. W. Trissl, C. Wilhelm, *Trends Biochem. Sci.*, 1993, **18**, 415.
41 S. C. Feifel, A. Kapp, R. Ludwig, F. Lisdat, *Angew. Chem. Int. Ed.*, 2014, **53**, 5676.
42 C. M. Silveira, M. G. Almeida, *Anal. Bioanal. Chem.*, 2013, **405**, 3619.
43 P. N. Ciesielski, C. J Faulkner, M. T. Irwin, J. M. Gregory, N. H. Tolk, D. E. Cliffel, G. K. Jennings, *Adv. Funct. Mater.*, 2010, **20**, 4048.
44 A. Mershin, K. Matsumoto, L. Kaiser, D. Y. Yu, M. Vaughn, M. K. Nazeeruddin, B. D. Bruce, M. Graetzel, S. G. Zhang,. *Sci. Rep.*, 2012, **2**, 234.
45 G. LeBlanc, G. Chen, E. A. Gizzie, G. K. Jennings, D. E. Cliffel, *Adv. Mater.*, 2012, **24**, 5959.
46 B. Munge, S. K. Das, R. Ilagan, Z. Pendon, J. Yang, H. A. Frank, J. F. Rusling, *J. Am. Chem. Soc.*, 2003, **125**, 12457.
47 N. Terasaki, N. Yamamoto, T. Hiraga, I. Sato, Y. Inoue, S. Yamada, *Thin Solid Films*, 2006, **499**, 153.
48 L. Frolov, Y. Rosenwaks, C. Carmeli, I. Carmeli, *Adv. Mater.*, 2005, **17**, 2434.
49 X. Yan, C. J. Faulkner, G. K. Jennings, D. E. Cliffel, *Langmuir*, 2012, **28**, 15080.
50 I. Carmeli, L. Frolov, C. Carmeli, S. Richter, *J. Am. Chem. Soc.*, 2007, **129**, 12352.
51 M. Ciobanu, H. A. Kincaid, V. Lo, A. D. Dukes, G. K. Jennings, D. E. Cliffel, *J. Electroanal. Chem.*, 2007, **599**, 72.
52 H. A. Kincaid, T. Niedringhaus, M. Ciobanu, D. E. Cliffel, G. K. Jennings, *Langmuir*, 2006, **22**, 8114.
53 B. S. Ko, B. Babcock, G. K. Jennings, S. G. Tilden, R. R. Peterson, D. E. Cliffel, E. Greenbaum, *Langmuir*, 2004, **20**, 4033.
54 A. Badura, D. Guschin, T. Kothe, M. J. Kopczak, W. Schuhmann, M. Rögner, *Energy Environ. Sci.*, 2011, **4**, 2435.
55 K. R. Stieger, S. C. Feifel, H. Lokstein, F. Lisdat, *Phys. Chem. Chem. Phys.*, 2014, **16**, 15667.
56 M. S. Artiles, C. S. Rout, T. S. Fisher, *Adv. Drug Delivery Rev.*, 2011, **63**, 1352.
57 Y. Wang, Z. Li, J. Wang, J. Li, Y. Lin, *Trends Biotechnol.*, 2011, **29**, 205.
58 S. M. Kaniber, F. C. Simmel, A. W. Holleitner, I. Carmeli, *Nanotechnol.* 2009, **20**, 345701.
59 M. Kato, T. Cardona, A. W. Rutherford, E. Reisner, *J. Am. Chem. Soc.*, 2013, **135**, 10610.
60 D. Gunther, G. LeBlanc, D. Prasai, J. R. Zhang, D. E. Cliffel, K. I. Bolotin, G. K. Jennings, *Langmuir*, 2013, **29**, 4177.
61 G. Chen, G. LeBlanc, G. K. Jennings, D. E. Cliffel, *J. Electrochem. Soc.*, 2013, **160**, H315.
62 G. LeBlanc , K. M. Winter , W. B. Crosby , G. K. Jennings, D. E. Cliffel, *Adv. Energy Mater.*, 2014, 1301953.
63 G. LeBlanc, E. Gizzie, S. Yang, D. E. Cliffel, G. K. Jennings, *Langmuir*, 2014, **30**, 10990.
64 T. Kothe, S. Pöller, F. Zhao, P. Fortgang, M. Röger, W. Schuhmann, N. Plumere, *Chem. Eur. J.*, 2014, 20, 11029.
65 C. Felder, J. Prilusky, I. Silman, J. Sussman, *Nucleic Acids Res.*, 2007, **35**, 512.
66 W. Humphrey, A. Dalke, K. Schulten, *J. Mol. Graph.*, 1996, **14**, 33.

Journal Name

RSCPublishing

ARTICLE